Hindawi
Advances in Civil Engineering
Volume 2022, Article ID 5469471, 16 pages
https://doi.org/10.1155/2022/5469471

Research Article

Displacement Characteristics of a Deep Excavation in Hangzhou Soft Clay

Yuan Mei,[1] **Lu Wang**,[1] **Dongbo Zhou**,[1] **and Liaoyuan Fu**[2]

[1]*Department of Civil Engineering, Xi'an University of Architecture and Technology, Xi'an, China*
[2]*Luoyang Rail Transit Group Co., Ltd., Luoyang, China*

Correspondence should be addressed to Lu Wang; imwlwl@163.com

Received 26 August 2021; Revised 15 January 2022; Accepted 24 February 2022; Published 16 March 2022

Academic Editor: Luigi Fenu

Excavations in a soft soil area are usually associated with substantial difficulties. Taking a special-shaped deep foundation pit in Hangzhou soft clay as the research object, the excavation performances, including groundwater level height, axial force, lateral wall, and soil deflection, and ground surface settlement were monitored and summarized based on the data published in the literature on similar excavations in Hangzhou, P. R. China. The following conclusions are drawn: (1) The axial forces of the struts dynamically change during the excavation and construction or removal of adjacent braces. (2) The ratio between the measured maximum wall deflection and excavation depth ($\delta_{h-\max}/H_e$) is 0.14–0.17%, larger than those in Shanghai. (3) The surface settlement behind the wall has an obvious primary influence zone and secondary influence zone, characterized by a "groove shape" and "triangle shape," respectively. The maximum ground surface settlement $\delta_{v-\max}$ ranges from 0.29% to 0.5% of the excavation depth. (4) The distribution of the ground settlement was analyzed. The relationship between the maximum settlements $\delta_{v-\max}$ is between 1.28 $\delta_{h-\max}$ and 3.72 $\delta_{h-\max}$. Moreover, ABAQUS software with Mohr–Coulomb soil models was used for model analysis of the construction process. The research results have important significance for the effective prevention of foundation pit accidents and the optimal design of deep foundation pit projects.

1. Introduction

Hangzhou is located on the lower reaches of the Qiantang River in southeast China, a superior position in the Yangtze Delta and only 180 kilometers from Shanghai. Geological sediments alternately accumulate and erode due to the influence of many marine transgression and regression events in Hangzhou, making Hangzhou foundation soil have low shear strength and high compressibility. Excavations in this area are usually associated with substantial difficulties; they may lead structural damage in the process of construction, such as the collapse of a foundation pit in 2021 and the sudden surge of foundation soil in Hangzhou Metro in 2016, as shown in Figure 1. Therefore, deep excavation in soft clays is still a hot topic of geotechnical engineering with high risk and difficulty. The monitoring data should be analyzed timely and in-depth to predict the deformation development law of deep foundation pit during the construction and take timely measures to control the risks in construction in advance to avoid accidents.

Many scholars conduct a detailed study on individual cases of deep excavation with extensive and comprehensive field monitoring data [1–6]; however, the shape of them is mostly strip. Researchers and engineers [7–15] have contributed a large number of field data to analyze the deformation characteristics and influencing factors of a foundation pit. In soft soil areas, scholars [2, 4, 16–20] have summarized the measured results of several deep foundation pits, obtaining the deformation characteristics of foundation pit retaining structures in soft soil and the ground surface settlement law. However, in-depth reports on deep excavations in the Hangzhou soft soil area are rather limited to date [14]. In engineering practice, a series of two-dimensional and three-dimensional finite element analyses [21–26] were used for model analysis and safety monitoring of the construction process of deep pits.

(a) (b)

Figure 1: Foundation pit accidents: (a) foundation pit collapse and (b) the sudden surge of foundation.

This study analyzes the deformation characteristics of a specially shaped deep foundation pit in Hangzhou soft clay including the underground water level, axial force, surface settlement, and lateral displacement of the retaining wall. ABAQUS software was used to simulate the excavation process of the foundation pit, and a comprehensive comparison and analysis with the measured data were simultaneously carried out. The field observations will be beneficial in a practical sense to researchers and designers.

2. Site Conditions

The investigated excavation is located in Xixi National Wetland Park, as shown in Figures 1 and 2. On the west side, 45 m away from the foundation pit is the Hangzhou Ring Expressway. There are no tall buildings or pipelines around the site.

The structure of the excavation is approximately 72 m long (axis direction) and 15 m wide and is divided into two zones: the south pit (SP) is 18 m deep, the north pit (NP) is 27.8 m deep, and the excavation depth of the foundation pit is 18.2–28 m. Considering the complex surrounding environment of the project, a diaphragm wall retaining structure with high rigidity and strength was adopted in the design concept. The cast-in-place diaphragm wall is 42 m deep, 1 m thick in the SP, and 1.2 m thick in the NP (see Figure 3). A top-down construction sequence and a composite strut system were adopted. The open excavation method (frame reverse method under the north area) is adopted for excavation. The first prop was cast using in situ reinforced concrete, and the remainder was prestressed steel props. The circular steel strut has an external diameter of 0.8 m and is 0.016 m thick, and the cross section of the rectangular concrete support is 0.8 m wide and 1 m high. Meanwhile, to reduce the impact of excavation on the environment, the foundation soil was improved within the range of 18.2 m to 22.2 m below the surfaces prior to excavation (see Figure 4).

2.1. Soil Parameters. Hangzhou has heavy rainfall, a high groundwater level, a wide distribution of soft clay, and a high groundwater content, which easily produces a large plastic flow and consolidation settlement. A series of field and laboratory tests were carried out on the soil quality of the project site. Combined with the static cone penetration test

Figure 2: Close view of the investigated excavation.

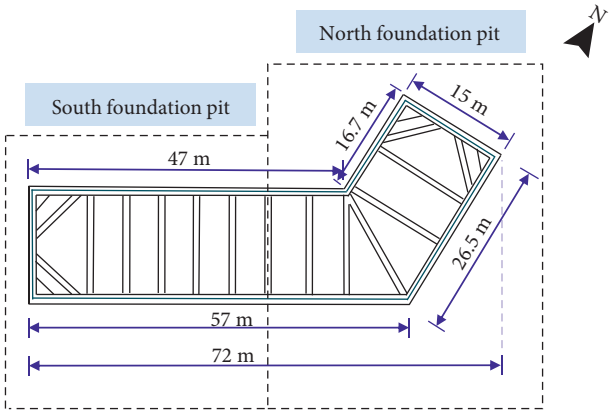

Figure 3: Plan view of the strut system.

curve, the soil layer exposed within the exploration depth range of the site is six layers, as shown in Figure 5.

The foundation pit was constructed using the top-down construction technique, together with diaphragm walls and struts as excavation supports. Major construction stages are defined in Table 1.

3. Test Program

Table 2 presents the main monitoring items and instruments installed on-site.

Each monitoring section is set with five settlement markers (DB 1 to DB 5), which are 4 m, 12 m, 24 m, 40 m, and 60 m away from the edge of the foundation pit. Five

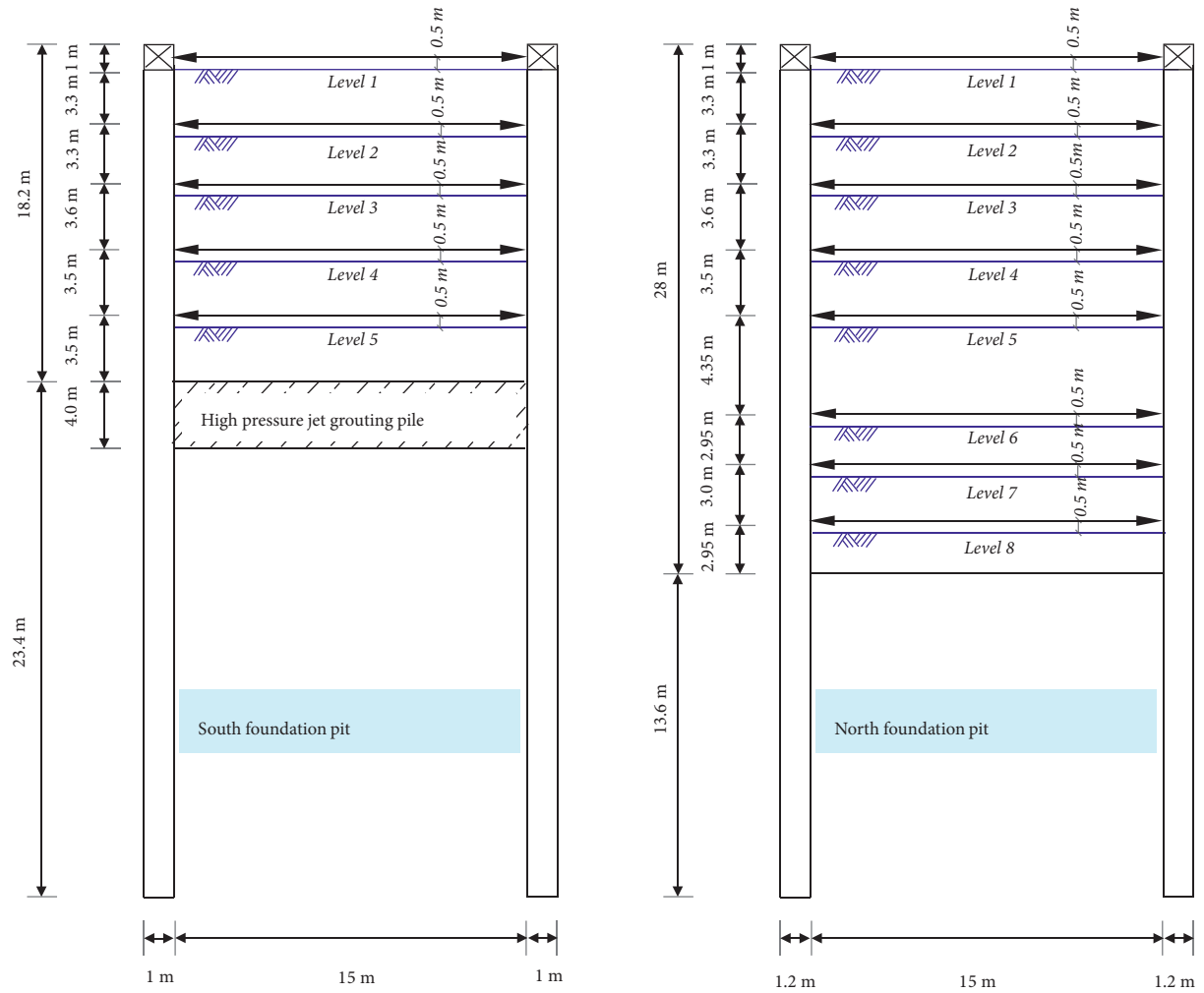

Figure 4: Cross section of the excavation.

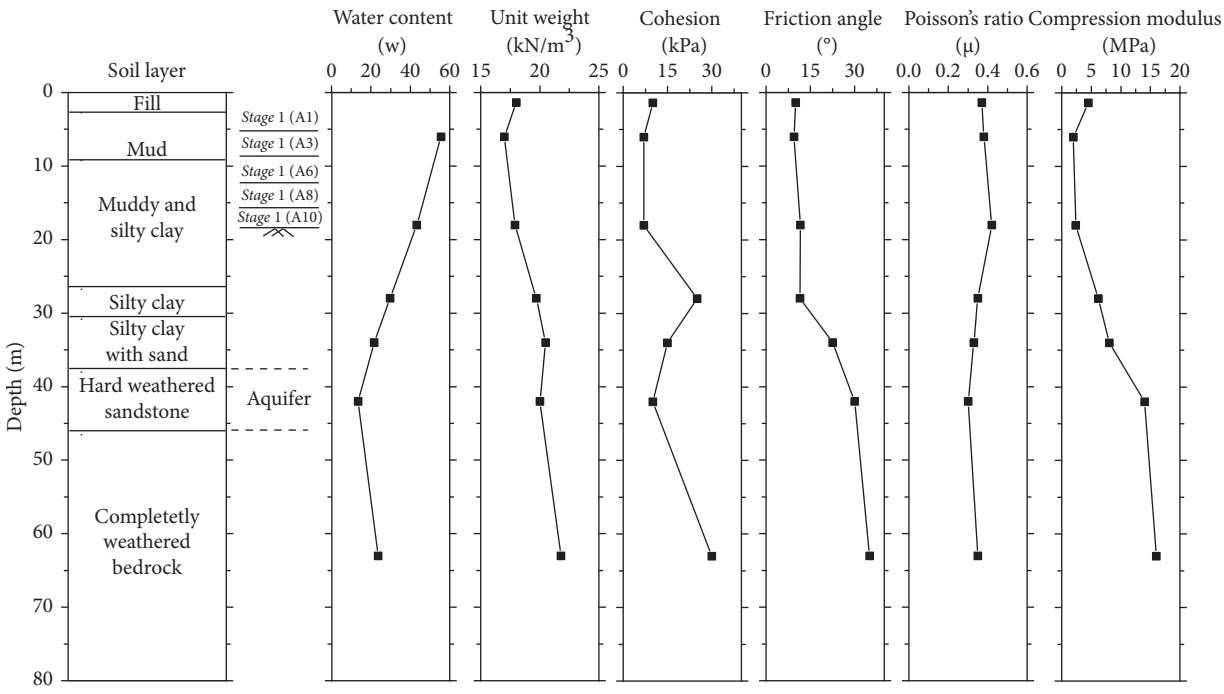

Figure 5: Soil profiles and material properties.

Table 1: Construction phases and sequence of the excavation.

Stage		Day	Construction activities
Preexcavation	O1	—	Construct diaphragm wall
	O2	—	Cast the first concrete prop 1
	O3	—	Construct high pressure jet grouting (−18.2 m −22.2 m)
Main excavation (I)	A1	1–8	Excavate to level 2 (−5.2 m)
	A2	9–13	Install prop 2, prestressed axial force
	A3	14–19	SP: excavate to level 3 (−8.5 m)
	A4	20–24	NP: cast the concrete prop 2 and waist beam
	A5	25–27	SP: install prop 3, prestressed axial force
	A6	28–34	Excavate to level 3 (−12.1 m)
	A7	35–37	Install prop 3, prestressed axial force
	A8	38–44	Excavate to level 4 (−15.65 m)
	A9	45–47	Install prop 4, prestressed axial force
	A10	48–57	Excavate to level 5 (−18.2 m)
	A11	58–60	Install prop 5, prestressed axial force
After excavation (II)	B1	61–92	SP: construct the second floor and reduce prop 5
	B2	93–119	SP: construct the first floor and reduce prop 2,3,4
	B3	120–125	SP: construct the roof of the first floor and reduce prop 1
	B4	61–94	NP: construct the second floor and reduce prop 4,5
	B5	95–150	NP: construct the first floor and reduce prop 1,2,3

Table 2: Overall layout of the instruments installed on-site.

Name of measuring point	Monitoring items	Instrument	Control value (mm)	Absolute value of alarm value (mm)
QX	Deep horizontal displacement of wall	Inclinometer	45	38
DB	Ground settlement	Leveling instrument	30	26
ZL	Axial force	Vibration wire gauge	—	—
SW	Groundwater level height	Steel ruler water level gauge	1000	500
TX	Deep horizontal displacement of soil	Inclinometer	60	51

groups of axial force meters are arranged for each layer of support (taking the first layer of the prop as an example, the axial force meter numbers are ZL 1–1~ZL 1–5). Five groups of axial force meters at the same plane position of the five layers of the strut form a monitoring section, for a total of five monitoring sections, as shown in Figure 6.

To ensure the safety of the foundation pit and predict the construction quality and water sealing effect of the diaphragm wall, the diaphragm wall cut off the confined water layer, so only the artesian well was set in the pit to drain the water (see Figure 6), and the groundwater level outside the excavation was monitored. The artesian wall goes deep into the hard weathered sandstone stratum. The hole diameter of the tube well/the diameter of the well tube is 800/300 mm, and the water level in the pit is controlled at 0.5~1 m below the excavation surface.

4. Observations

4.1. Variation Law of the Groundwater Level. The groundwater is a key element in almost every construction project [27]. Through continuous monitoring of the water level outside the pit for nearly six months, the change in the groundwater level outside the pit with the construction time of the foundation pit was obtained, as shown in Figure 7. It can be seen from the figure that the fluctuation of the groundwater level is strong. Due to timely precipitation and other measures, there were no accidents in the construction of the foundation pit. The records also show that the water levels in the two places marked in Figure 7 exhibit a rapid upward trend due to rainfall. In the excavation stage, the cumulative change in the groundwater level around the pit also increases, and the groundwater level shows a downward trend except at SW 4. Finally, the water level of the foundation gradually tends to be stable, and there is no large change in the water level. This is due to the good anti-seepage effect of the diaphragm wall and the waterproof curtain. In addition, the main soil layer at the depth of the foundation pit is muddy, soft soil, and its permeability is very low. In the process of excavation, the change in the water level indirectly reflects the prop strength of the retaining structure. Therefore, in foundation pit monitoring, when the water level has a large change, attention should be paid to the monitoring of the settlement around the foundation pit.

4.2. Variation Law of Support Axial Force. With increasing excavation depth, the steel strut was gradually erected. Figure 8 presents the variation curve of the axial force of the

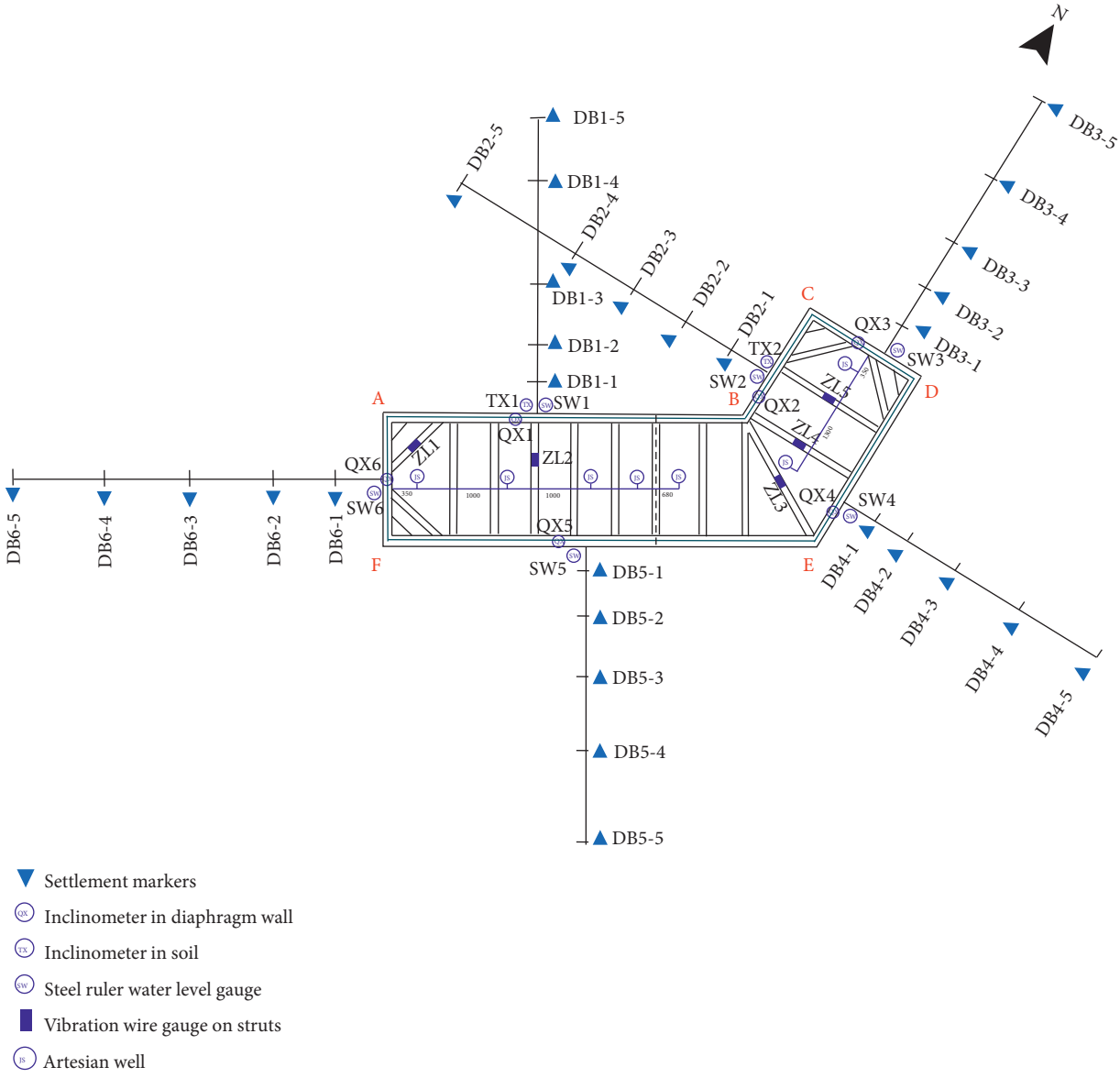

Figure 6: Monitoring layout of the foundation pit.

first layer concrete of prop ZL 1~ZL 5 with respect to time. The development trend of the axial force was relatively similar, and the fluctuation tended to be stable after reaching a maximum value 2~3 weeks after pouring. The axial force monitoring value of ZL 3 at the corner of the foundation pit was the largest, which indicated that the external load induced by excavation was mainly borne by ZL 3, while the axial force monitoring value of ZL 1 at the corner of the foundation pit was the smallest and changed gently, and the spatial effect of the structure was obvious, which corresponds to the deep horizontal displacement of the wall. In the process of excavation, the first strut showed an increasing trend with excavation depth, which illustrated that the active earth pressure increased, and the force shared by the two struts gradually increased, consistent with the increasing trend of the struts. After the arrangement of the second prop, it shared the pressure of the pit side soil, resulting in a decrease in the axial force of the first prop. At the same time, in the process of support removal, the removal of each strut will also have a great impact on the axial force of the adjacent strut. Thus, the impact of mutation on the prop should be fully concentrated in the design.

4.3. Lateral Wall and Deep Soil Displacement. Figures 9 and 10 show the observed lateral movement profiles of the diaphragm wall at each side of the excavation area. Jamsawang et al. [16] suggested that the inclinometer readings are reliable when the tip of the inclinometer is properly embedded into a stable stratum. In this project, the inclinometer burial depths of the diaphragm and soil are 42 m and 44 m, respectively, which were deeply inserted into the stable stratum located in the completely weathered bedrock; hence, toe movement was not obvious. The wall deflection first behaved in a positive fashion and then gradually changed to a cantilever model; that is, the overall performance was

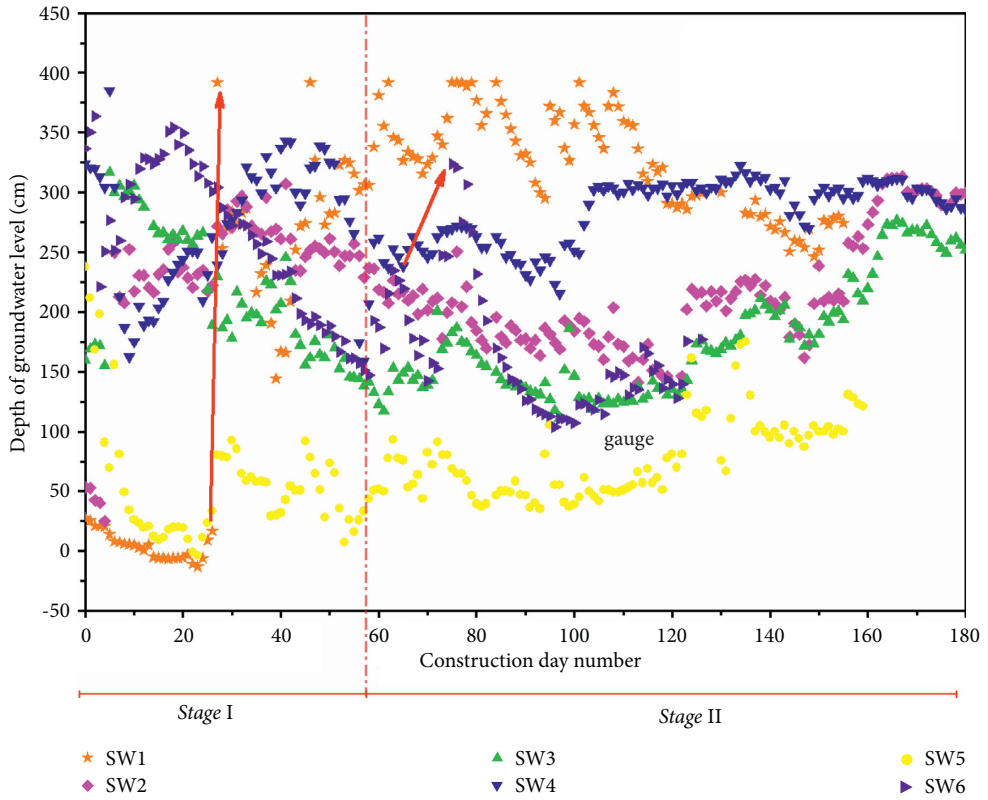

Figure 7: Monitoring of the groundwater level outside the excavation.

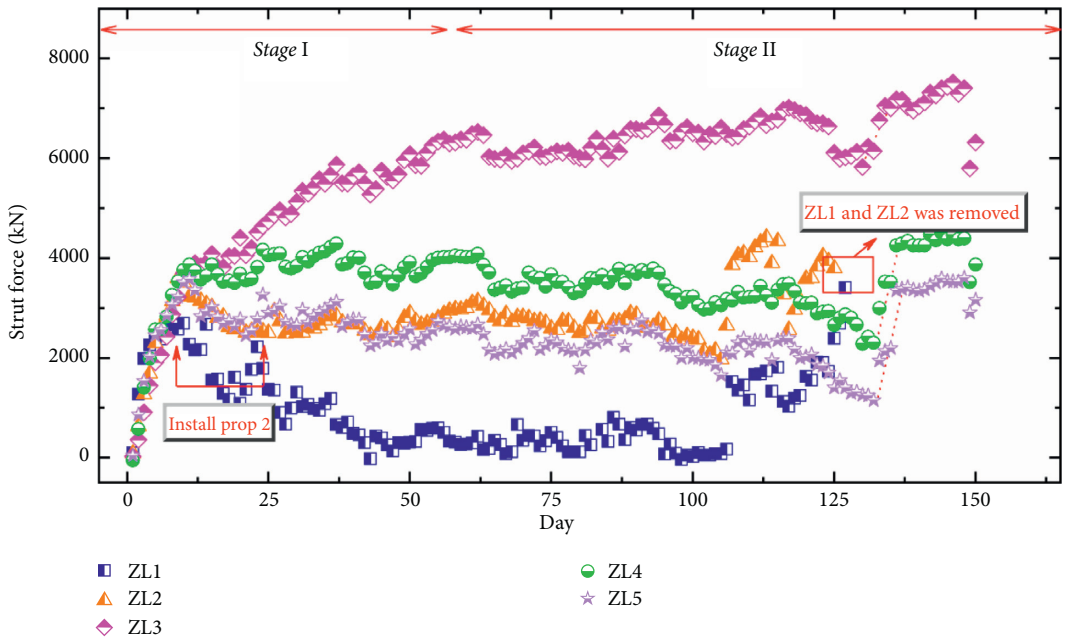

Figure 8: Variation law of the support axial force.

composite deformation, mainly due to the larger depth of the retaining structure in the soil and other reasons. The maximum horizontal displacement of each measuring point greatly increased, which indicated that with the excavation of the soil in the pit, the active earth pressure behind the wall increased continuously, resulting in an increase in the horizontal displacement of the retaining structure. The deformation values of the QX 3 and QX 6 measuring points near the corner of the foundation pit were less than 20 mm, which were significantly smaller than that of the middle of the pit, and the difference was approximately 30%~40%. This is mainly because the horizontal stiffness of the short side of

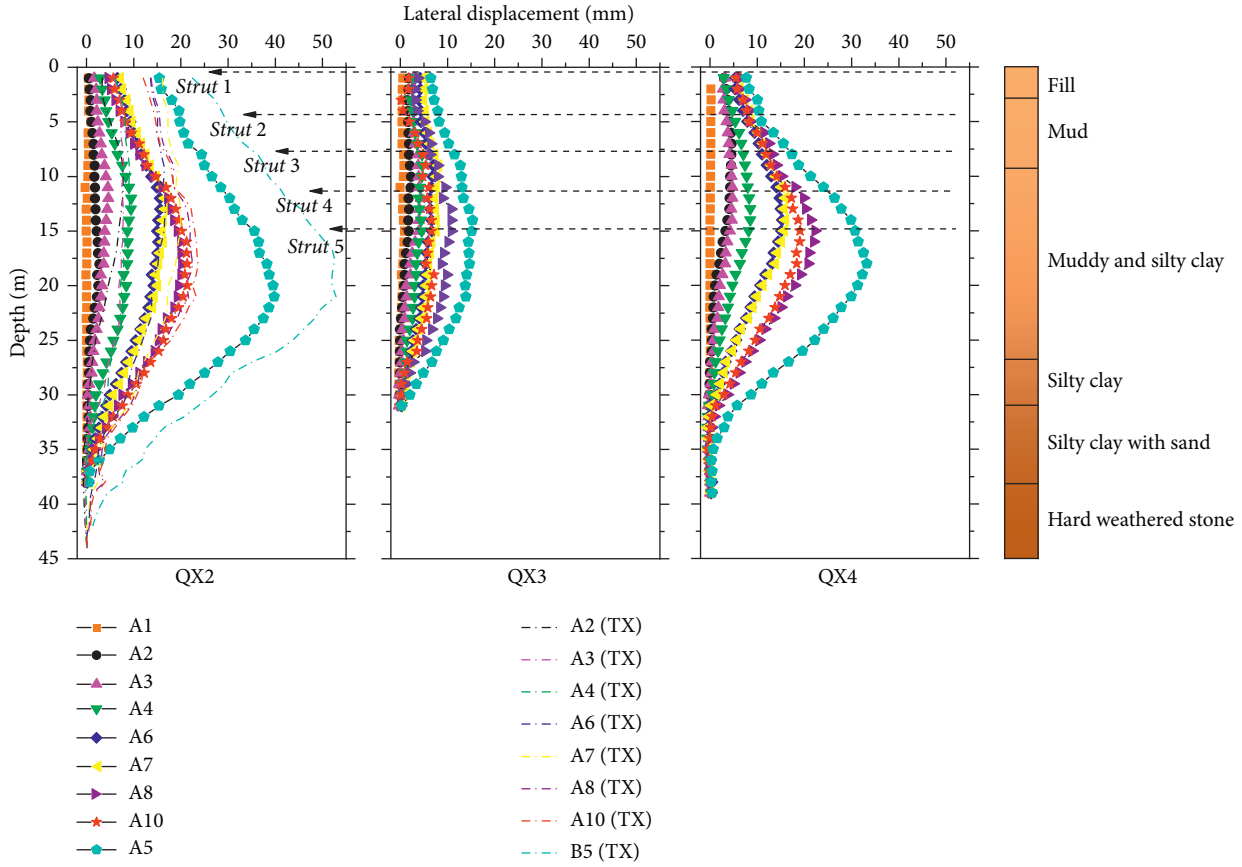

Figure 9: Lateral displacement of the diaphragm wall in NP.

the pit inhibits the development of the deformation, which illustrates that the restraint effect of the rigid diagonal brace on the diaphragm wall is evident [25], and only the continuous slab, which has a horizontal bearing capacity, like the diaphragm wall, can produce a deformation inhibition effect at the corner of the excavation, which has an obvious spatial effect. The maximum deformation of the long side of the wall is approximately 39.82 mm, which occurs at a depth of 21 m. The maximum deformation of the short side continuous wall of the foundation pit is approximately 15.34 mm. The ratio of the maximum deformation of the long side of the pit to the maximum deformation of the short side is 2.6 times. The maximum deformation of the wall at the mid-span of the long side of the pit is evident.

Ou et al. [28] proposed that the maximum lateral displacement depth of the wall in each stage of the foundation pit excavation generally occurs near the excavation surface, that is, $H_m = H$, where H_m is the maximum lateral displacement depth of the retaining wall. Shanghai clay H_m/H_e is slightly greater than 1.0 [29]. In the Hangzhou clay area, the maximum lateral displacement depth is between 4 m above the excavation surface and 7 m below the excavation surface. When the excavation depth is shallow ($H \leq 10$ m), the maximum lateral displacement depth is below the excavation surface. As excavation continued, the depth of the maximum horizontal displacement of the retaining structure gradually moved downwards, and the final maximum lateral displacement point depth was basically near the excavation face, that is, $H_m \approx H$. When the excavation reaches the base, the maximum displacement of the SP wall occurs at measuring point QX 1, which is 30.65 mm at a depth of 22 m, or approximately 0.17% of the excavation depth. SP occurs at measuring point QX 2, which is 21.37 mm at a depth of 18 m, or approximately 0.12% of the excavation depth. Due to the soil distribution and type of supporting structure, it is slightly smaller than the conclusion that δ_{h-max}/H is between 0.23% and 1.71% of the excavation in the Hangzhou clay area, as described by Ying et al. [30].

The horizontal displacements of QX1 and QX2 are also indicated in Figure 10. The change and development law of the lateral displacement of the soil is generally consistent with the diaphragm wall; however, the lateral displacement of the soil under various working conditions is larger than that of the continuous wall.

4.4. Surface Ground Settlements. Figure 11 shows the surface settlement monitoring curve for each measuring point in the SP and NP. The surface settlement behind the wall is in the form of grooves and triangles, and there are evident main influence areas, I (the distance to the pit edge is less than 0.75 H, H is the height of the retaining wall), II (the distance to the pit edge is $(0.75H \sim 0.5H)$, and III (the distance to the pit edge is more than 5H). Therefore, the main influence area I is drawn in Figures 11 and 12 for comparison, and it can be observed that the main influence area of this case is generally located in the 0.75 H area. At the end of excavation (i.e.,

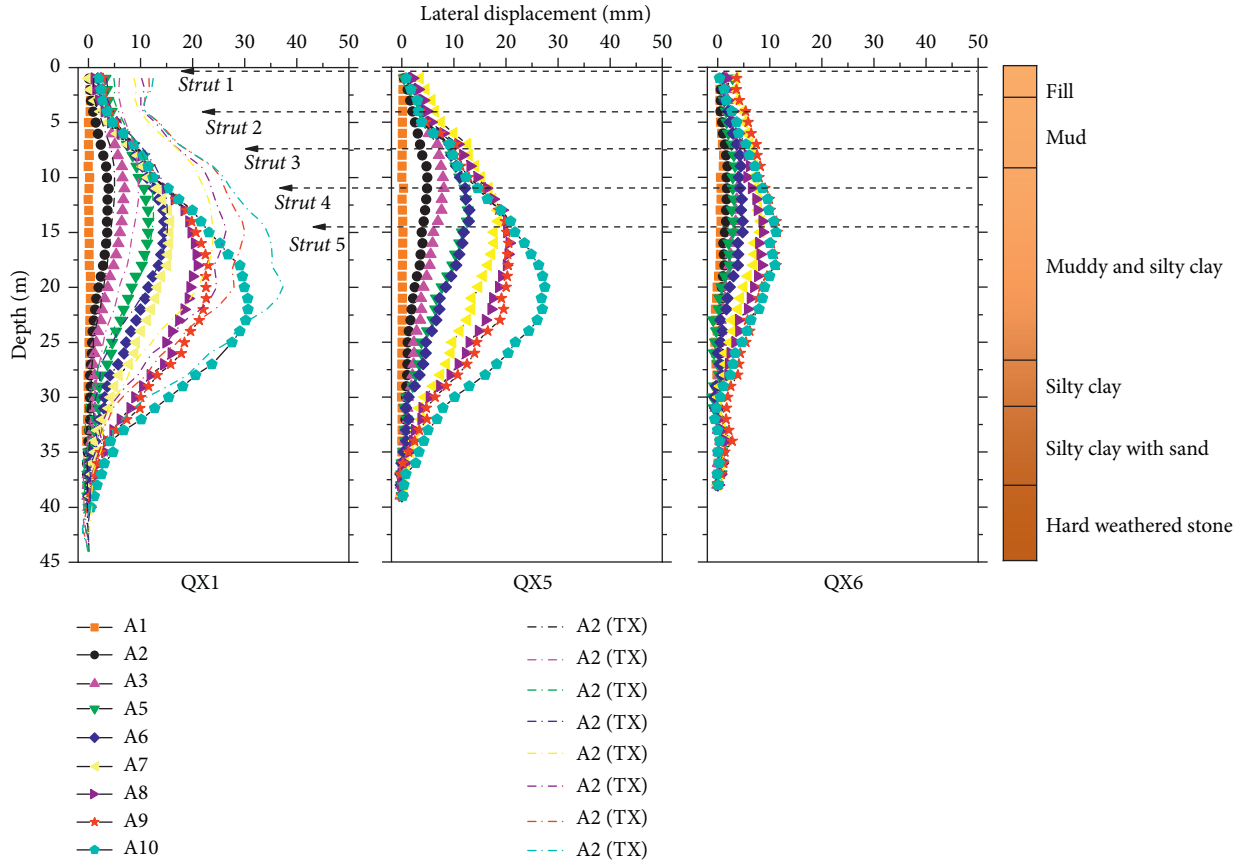

Figure 10: Lateral displacement of the diaphragm wall in SP.

stage I), the maximum surface subsidence of SP is 51.97 mm, which occurs at the DB 1 measuring point 4 m away from the edge of the foundation pit; the maximum surface settlement of NP is 50.84 mm, which occurs at the DB 12 m away from the edge of the pit, and the difference between them is nearly 100%, both exceeding the red alarm control value of 30 mm. The influence range of the intermediate and final conditions of SP and NP can reach 40 m beyond the pit wall, which is more than twice the excavation depth. The location of the maximum ground subsidence behind the wall is not more than 1.3H. The short side on both sides is long, the surface subsidence is small, and the maximum settlement occurs 24 m away from the foundation pit; in general, the pit angle effect is obvious. Clough proposed that the distribution form of the surface settlement curve outside the foundation pit has a strong relationship with the amount of settlement. When the amount of settlement is large, it is triangular, and when the amount of settlement is small, it is parabolic. Except for DB 1 (SP) and DB 4 (NP), which are triangular settlement profiles, the other measuring points are parabolic settlement profiles. After the completion of the main structure, the settlements of DB 1 and DB 4 are 89.54 mm and 69.96 mm, respectively, consistent with the conclusion of Clough [31].

To further study the influence scope of foundation pit excavation, Figure 13 shows the distribution of the ground settlement behind the wall of the foundation pit. The horizontal axis is the ratio of the distance from a point behind the wall to the excavation depth (d/H_e), and the vertical axis is the dimensionless surface settlement (the ratio of the settlement of a point to the excavation depth, which is a percentage). In addition, published measured data from foundation pit engineering in Hangzhou are added for comparative analysis. As shown in Figure 13, the measured surface settlement effect in this area can be divided into two parts: the stable zone of $0 \le d/H_e \le 1.32$ and the linearly decreasing zone of $1.32 \le d/H_e \le 3.5$, where δ_v decreases with increasing $1.32 \le d/H_e \le 3.5$, are located in the envelope line of the Hangzhou foundation pit, as described by [14]. It can also be seen that the settlement of the Hangzhou area is larger in the range of $0 \le d/H_e \le 1.5$. It should be noted that this paper does not compare with the classical Peck curve for predicting the relationship between the surface settlement and the distance from the pit wall because Peck [32] obtained the above rule according to a foundation pit with sheet pile as the main prop in hard soil layer, and the land settlement is relatively large. In this case, the diaphragm wall in clay is used as the supporting foundation pit, the design and construction level of the supporting system are greatly improved compared with the excavation engineering described by Peck [32], and the deformation control is also stricter.

4.5. Relationship between Ground Settlement and Lateral Displacement. The horizontal displacement of the wall is related to the surface settlement. As shown in Figure 14, the area bounded by the surface settlement profile and the abscissa

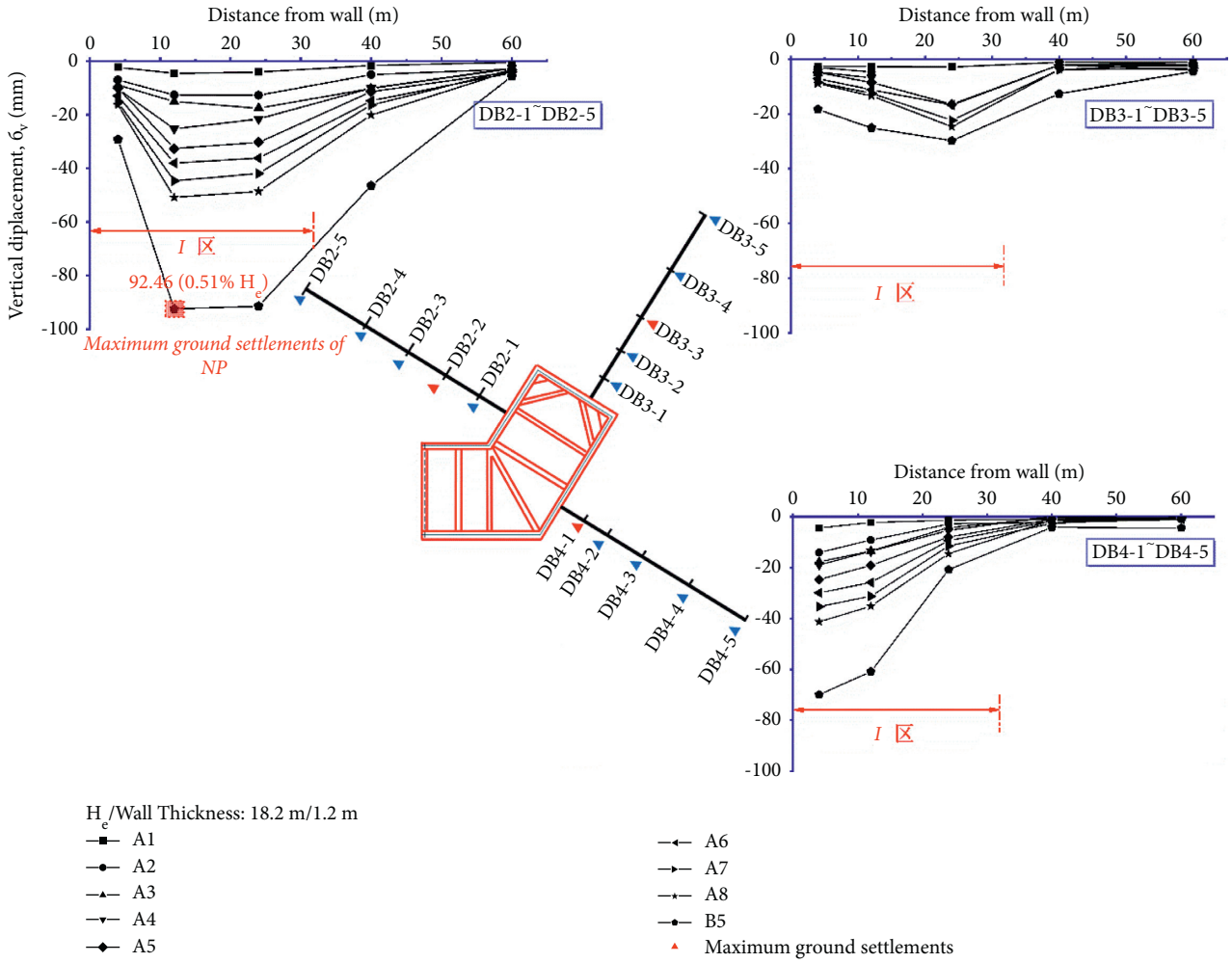

Figure 11: Ground surface settlements of NP.

may be regarded as the incremental volume loss of the retained ground (V_s), and the area bounded by the diaphragm wall displacement profile and the abscissa represents the volume gain of the retained ground (V_w). Milligan [33] suggested that the lateral displacement area of the wall is approximately equal to the surface settlement area behind the wall, while Bowles [34] proposed that the surface settlement area behind the wall is approximately 1.33 times the lateral displacement area of the wall. In Figure 14, V_s is much larger than V_w, indicating that it does not conform to the conclusion of Milligan [33]. and the typical assumption of constant-volume deformation in soft clays is not applicable for this site [4].

The excavation of the foundation pit leads to an imbalance in earth pressure, which drives the retaining wall to deform into the pit. At the same time, the soil behind the wall produces settlement deformation, so as to obtain a new balance. Therefore, settlement and lateral displacement are closely related. Figure 15 compares the relationship between the surface deformation and lateral displacement of the wall. In the main excavation stage, the ratio of the maximum surface settlement to the maximum lateral displacement of the wall () is roughly between $\delta_{v-\max} = 1.28\delta_{h-\max}$ and $\delta_{v-\max} = 3.72\delta_{h-\max}$. Many scholars have previously studied the relationship between $\delta_{v-\max}$ and $\delta_{h-\max}$. Clough considered whether it is sandy soil, hard clay, or soft clay, where $\delta_{v-\max} = (0.5 \sim 1.5)\delta_{h-\max}$; Mana and Clough [35] supposed the foundation pit in clay stratum $\delta_{v-\max} = (0.5 \sim 1.0)\delta_{h-\max}$; the statistics of 10 foundation pits described by Ou et al. [11] show that $\delta_{v-\max}$ mostly decreases in $(0.5 \sim 1.0)\,\delta_{h-\max}$; the statistical results of Moormann [36] show that there is generally $\delta_{v-\max} = (0.5 \sim 2.0)\delta_{h-\max}$ in soft clay; Wang et al. [12] collected and analyzed the wall displacement and ground subsidence caused by deep excavation of soft soil in Shanghai and concluded that $\delta_{v-\max}/\delta_{h-\max}$ is generally between $\delta_{v-\max}/\delta_{h-\max}$; Xiao et al. [19] analyzed 92 examples of soft soil from foundation pits in China and concluded that $\delta_{v-\max}/\delta_{h-\max}$ is generally between 0.5 and 2.5; after analyzing the deep soft clay foundation in Hangzhou, Ying et al. [14] found that $\delta_{v-\max}/\delta_{h-\max}$ is generally between, and the research results in this paper are greater than the statistical results of the above researchers. It is speculated that the settlement value of soil is greater than the past statistical results due to the existence of muddy soil. In general, from the comparative statistical data, the relationship between the surface settlement and the lateral deformation of the diaphragm wall is affected by many factors.

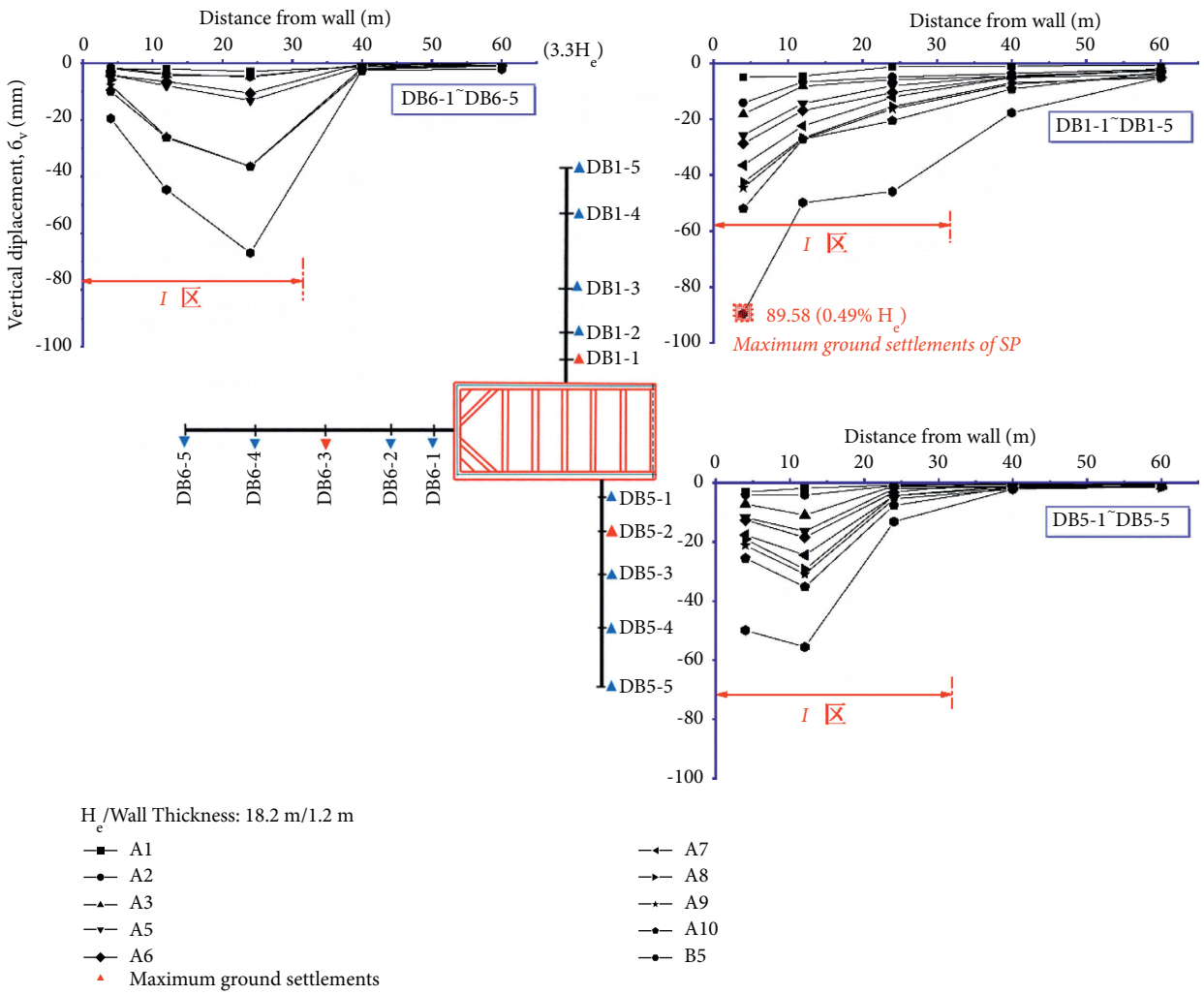

Figure 12: Ground surface settlements of SP.

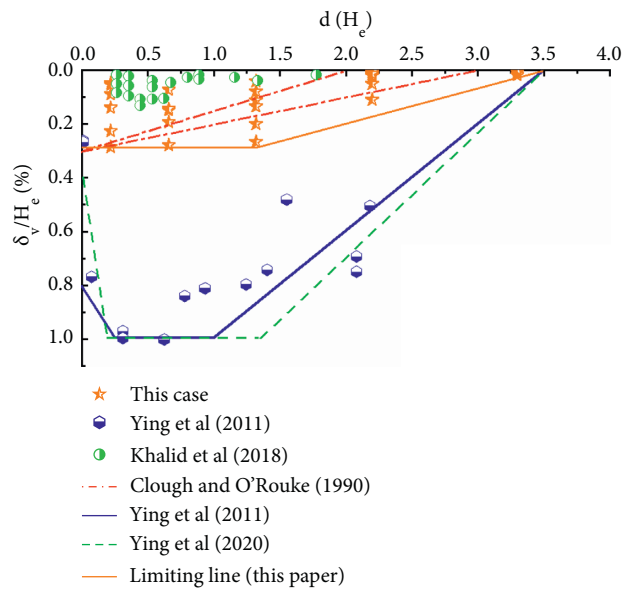

Figure 13: Relationship between the relative settlement and the normalized distance from the wall.

5. Numerical Analysis of the Field Case Study

5.1. Modeling. Numerical simulation is an effective approach to study the soil structure interaction mechanism of deep foundation pits. Due to limitations in software and computing resources, two-dimensional simulation (plane strain and axisymmetric analysis) is widely used in the design of deep foundation pits. However, two-dimensional analysis cannot consider the corner effect, which indicates that the wall deformation and ground movement near the corner are smaller than those around the center of the wall. In addition, compared with the simplified three-dimensional symmetrical square or rectangular analysis, two-dimensional plane strain analysis often overestimates the wall deflection and ground settlement behind the wall [22]. A classical model (Mohr–Coulomb model) was coded in ABAQUS and adopted for the numerical simulation based on the above analysis. To avoid boundary effects, the model size is 170 m × 140 m × 100 m (length × width × depth); see Figure 16. The coupling effect with groundwater is not considered since the dewatering treatment was carried out before excavation of the foundation pit. According to the

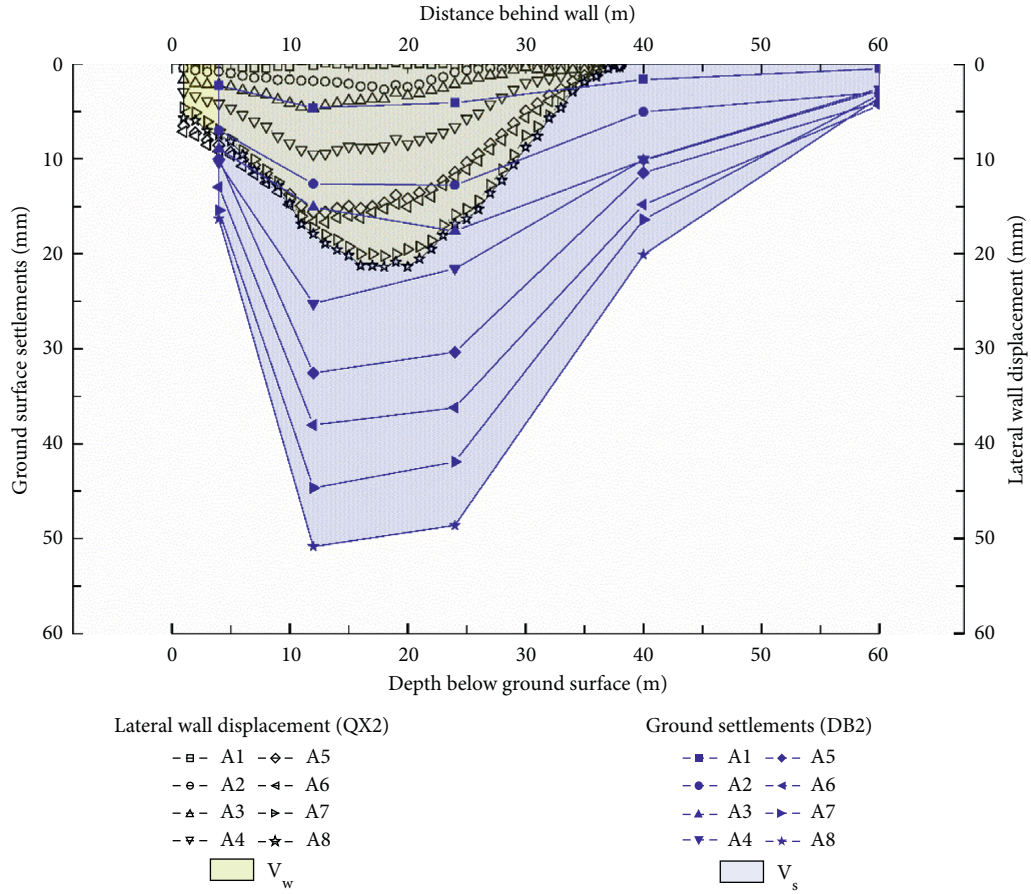

Figure 14: Relationship between the ground surface settlement and lateral wall displacement during excavation.

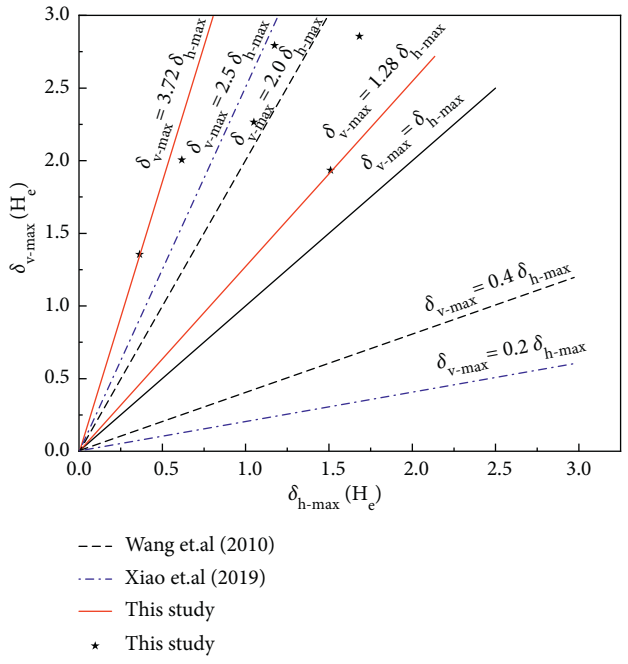

Figure 15: Relationship between the maximum ground settlement and maximum displacement of retaining wall.

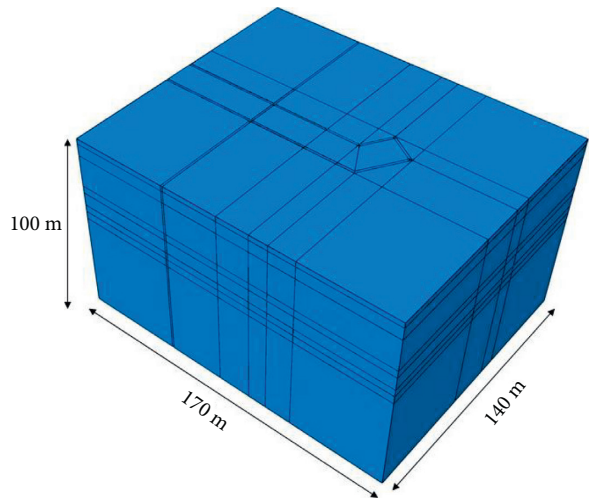

Figure 16: Finite element analysis model.

field exploration results, some soils with similar properties are combined and considered homogeneous soil, and the soil in the area where the foundation pit is located is divided into seven layers. In the simulation, the excavation of the foundation pit is simplified to some extent. In the actual

project, five layers are excavated in the SP and seven layers are excavated in the NP. This simulation process is only the key construction stage, that is, only five layers of soil are excavated in SP and NP.

The upper surface of the model is a free surface; the left and right sides of the model are constrained by X-direction displacement; the front and rear sides of the model are constrained by Y-direction displacement; and the lower part is constrained by X-, Y-, and Z-direction displacement.

When the diaphragm wall is constructed with the trench wall method, excavation of the soil in the trench section will cause a disturbance and stress release of the surrounding soil and produce a certain soil displacement. According to the research of Ng et al. [37]; the lateral stress of the soil in the trench section of the diaphragm wall will be reduced, but it will return to the initial K_0 lateral pressure state after the concrete is poured; therefore, the surface settlement and stress release caused by continuous wall trench construction is also ignored in this analysis. The concrete support and diaphragm wall are made of C35 reinforced concrete. According to the data of the American Concrete Institute, the elastic modulus of concrete can be estimated by [24]

$$E = 4700\sqrt{f_c'}\,(MPa). \tag{1}$$

The physical and mechanical parameters of the support structure are given in Table 3.

The tie constraint is often used to simulate the connection between the bracing and diaphragm wall. However, in practical engineering, the connection between the bracing and diaphragm wall may not be rigid and may rotate and produce gaps. These reasons may lead to large displacements of the surrounding soil during simulation. There are great differences in stiffness and strength between the diaphragm wall and soil. Under the action of an external force, the interface between the diaphragm wall and soil may produce relative sliding or detachment. Therefore, the interface element is set between the diaphragm wall and soil in the finite element numerical analysis model. The contact between the soil and wall is surface-to-surface contact. The normal stiffness and tangential stiffness are limited in the contact properties. The normal stiffness adopts a hard contact and allows the continuous wall surface to penetrate into the external soil layer or separate from the adjacent soil layer. That is, the contact pressure that can be transferred between the contact surfaces is unlimited. The distance between two surfaces is called the gap. When the gap between two surfaces becomes zero, it is considered that two surfaces have come into contact, and contact constraints are imposed on the corresponding nodes. For the tangential action, the penalty function is selected for the tangential stiffness, and the friction coefficient of the contact surface is 0.176.

5.2. Numerical Results and Comparisons with Measurements. The measured values and finite element calculation results (see Figure 17) of QX 5 and DB 5 of the retaining wall in the key construction stage are selected, and the comparison curve of the monitoring value and the calculation value of the retaining wall are shown in (Figure 18).

Due to the limited number of monitoring points and the discreteness of the monitoring results, there must be errors between the monitoring results and the calculation results. Through comparative analysis, however, it can be seen that the wall deformation law obtained by finite element analysis is consistent with the measured wall deformation law, which indicates that the ground settlement law determined by computational aid provides reliable results. The difference between the calculated and measured deformation of the maximum diaphragm wall at QX 5 is 22.7 mm, which is different from the conclusion that the calculated displacement of the diaphragm wall using the Mohr–Coulomb model is less than the measured value obtained by Likitlersuang et al. [38], and the difference between the maximum surface settlement and the measured value is 8.03 mm, which is approximately 22% of the measured value.

The settlement of the surrounding soil obtained by the finite element method is consistent with the experimental field measurements, and the maximum settlement position is more accurate, which reflects well on the deformation law of the surrounding soil in the process of foundation pit excavation, but the measured surface settlement value is smaller than the finite element calculation result. The numerical simulation cannot account for the disturbance of construction machinery, space-time effect, and many other uncertain or variable factors, resulting in a certain deviation between the calculated value and the monitoring value, but the numerical simulation can provide a certain theoretical basis for the design of foundation pit retaining structures, verify the design scheme, and guide the construction to a certain extent. The Mohr–Coulomb model can describe the plastic deformation of soil and reflect the failure behavior of soil, but its stress-strain relationship before failure is linear elastic, so it cannot describe the nonlinear deformation behavior of soil well or consider the influence of the stress path on the mechanical characteristics of soil.

6. Discussions

The water head difference inside and outside the foundation pit increases with excavation depth. Under this situation, the groundwater outside the pit will bypass the bottom of the diaphragm wall and flow into the foundation pit. If the drainage in the foundation pit is too slow, then it will cause water accumulation in the pit. To ensure construction of the foundation pit in the "dry" state, drainage of the foundation pit should be performed in time. The rainy season will affect the water level change of the foundation pit. If the construction is in the rainy season, then sufficient pumping equipment must be kept prepared, and the drainage and interception of the foundation pit must be constructed well. To avoid bottom displacement of the inclinometer, the inclinometer should be inserted into the hard soil layer. Figure 6 clearly shows that the upper part of the retaining wall at the end of the excavation of NP shows a "cantilever" displacement. It is speculated that untimely erection of the support leads to a long exposure time of the soil and a large

Table 3: Physical and mechanical parameters of the support structure.

Structure	Density (kN·m^{-3})	Poisson's ratio (μ)	Young's modulus (E/GPa)	Elements
Soil		See Figure 5		C3D8R
Diaphragm wall	2500	0.2	28	C3D8R
Steel support	7800	0.3	200	B32
Reinforced concrete support	2500	0.2	28	B32

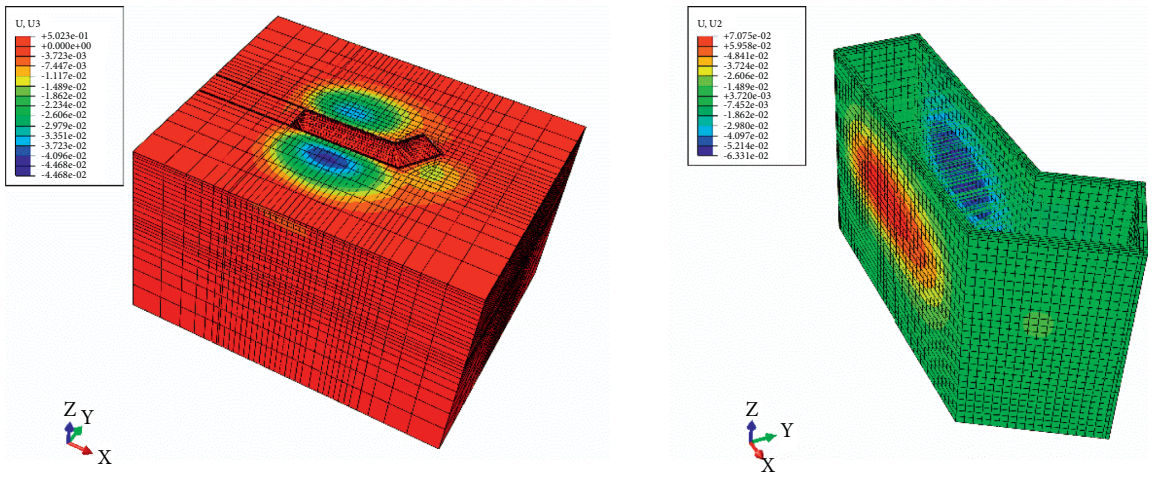

Figure 17: Finite element calculation results: (a) surface settlement and (b) diaphragm wall.

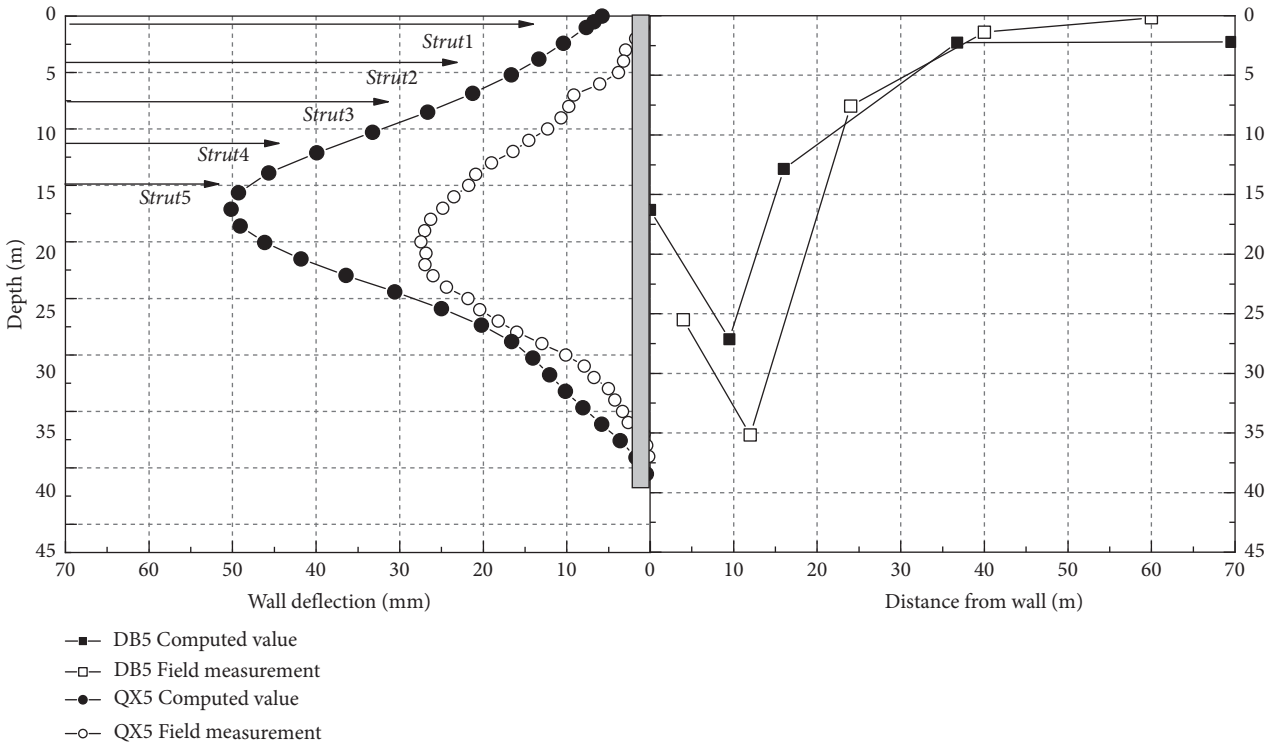

Figure 18: Comparison of the measured and simulated values.

displacement of the pile top. Timely installation of the first support plays a very important role in the control of deformation. The lateral displacement of the short side of the retaining wall is significantly smaller than that of the long side, and the spatial effect is obvious. When excavating in soft soil areas, we must consider reasonable support settling and the spatial effect of foundation pits to maximize the role of the support.

In this paper, the temperature effect of bracing is not considered in the analysis of the three-dimensional finite

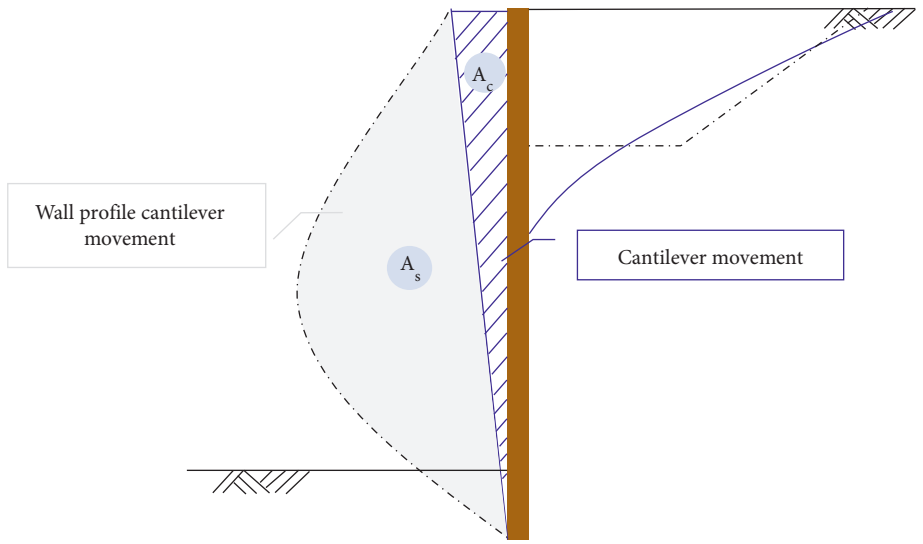

Figure 19: Diagram of cantilever movement and wall profile cantilever movement.

element method, and the constitutive model is relatively simple, so it is difficult to simulate the change in the foundation pit. However, in the actual design, it is difficult to realize a detailed model of all the characteristics related to the construction of deep foundation pits in the model, so more sensitive parameters should be studied in-depth. Ways to evaluate the influence of these complex factors on the deformation of foundation pits in numerical analysis require further study.

The surface settlement behind the foundation pit wall has an obvious main influence area and secondary influence area, and the influence area of SP and NP can reach 60 m outside the pit. With the increasing excavation depth of the foundation pit, the surface settlement increases, especially in the main construction stage. The settlement of DB4 in SP and DB1 in NP is larger than that of other measuring points, and the surface settlement behind the wall is a "triangle". However, it is speculated that another reason may be related to the cantilever deformation (A_c) of the diaphragm wall and saddle-shaped lateral displacement area (A_s) proposed by Ou [39]. As shown in Figure 19, when $A_s \geq 1.6A_c$, the surface settlement presents a saddle shape, and vice versa.

7. Conclusions

Based on the field monitoring and numerical simulation of special-shaped deep foundation pits, the following conclusions can be drawn through the above comparative analysis:

(1) As the main retaining structure, the diaphragm wall is not only used to resist the earth pressure behind the wall but also has a certain anti-seepage effect. The change in the water level indirectly reflects the support strength of the retaining structure. Therefore, in the monitoring work of foundation pits, when the water level changes greatly, we should pay close attention to the monitoring of the settlement around the foundation pit.

(2) The results of the numerical calculation and field monitoring show that the lateral deformation of the long side and short side of the diaphragm wall presents a saddle shape during the excavation of the special-shaped deep foundation pit in the soft soil area, the position of the maximum deformation gradually moves downwards, and the ratio of the maximum deformation of the long side to the maximum deformation of the short side of the foundation pit is 2.6 times. After excavation, the maximum displacement $\delta_{h-\max}$ of the retaining wall occurs at measuring point QX 2, which is approximately 40 mm, and the $\delta_{h-\max}/H_e$ of the foundation pit is between 0.14% and 0.17%. The deformation of the midpoint section of the long side of the foundation pit is large, and the spatial effect of the foundation pit is obvious.

(3) The distribution pattern of surface settlement behind the wall is determined, and the envelope of surface settlement behind the wall is given. In this paper, the ratio of the maximum surface settlement to the maximum lateral displacement of the wall (i.e., $\delta_{v-\max}/\delta_{h-\max}$) is roughly between $\delta_{v-\max} = 1.28\ \delta_{h-\max}$ and $\delta_{v-\max} = 3.72\delta_{h-\max}$ [40].

Data Availability

No data were used to support this study.

Conflicts of Interest

The authors declare that they have no conflicts of interest.

Acknowledgments

The research described in this paper was financially supported by the Shaanxi Provincial Key Research and Development Project (Grant no. 2020SF-373), the Shaanxi

Provincial Department of Education Special Scientific Research Program Project Fund (Grant no. 17JK0424), and the Xi'an Science and Technology Program Project (Grant no. 20180591SF18SF25).

References

[1] H. H. Chen, J. P. Li, and L. Li, "Performance of a zoned excavation by bottom-up technique in shanghai soft soils," *Journal of Geotechnical and Geoenvironmental Engineering*, vol. 11, Article ID 05018003, 2018.

[2] R. J. Finno, L. G. Arboleda-Monsalve, and F. Sarabia, "Observed performance of the one museum Park west excavation," *Journal of Geotechnical and Geoenvironmental Engineering*, vol. 141, Article ID 04014078, 2015.

[3] B.-C. B. Hsiung, "Observations of the ground and structural behaviours induced by a deep excavation in loose sands," *Acta Geotechnica*, vol. 15, no. 6, pp. 1577–1593, 2020.

[4] C. W. W. Ng, Y. Hong, G. B. Liu, and T. Liu, "Ground deformations and soil-structure interaction of a multi-propped excavation in Shanghai soft clays," *Géotechnique*, vol. 62, no. 10, pp. 907–921, 2012.

[5] C. Y. Ou, B. Y. Shiau, and I. W. Wang, "Three-dimensional deformation behavior of the taipei national enterprise center (TNEC) excavation case history," *Canadian Geotechnical Journal*, vol. 37, pp. 438–448, 2000.

[6] X. Zhao, G. Zhou, L. Qiao, and Y. Chen, "Behaviors of wall and ground due to T-shaped excavation," *KSCE Journal of Civil Engineering*, vol. 23, no. 1, pp. 1–10, 2019.

[7] M. Ehrlich and R. C. Silva, "Behavior of a 31m high excavation supported by anchoring and nailing in residual soil of gneiss," *Engineering Geology*, vol. 191, no. 5, pp. 48–60, 2015.

[8] N. K. Hung and N. Phienwej, "Practice and experience in deep excavations in soft soil of ho chi minh city, vietnam," *KSCE Journal of Civil Engineering*, vol. 20, no. 6, pp. 2221–2234, 2016.

[9] T. Masuda, *Behavior of Deep Excavation with Diaphragm wall*, Massachusetts Institute of Technology, Cambridge, Massachusetts, 1993.

[10] Y. Mei, Y.-L. Li, X.-Y. Wang, J. Wang, and C.-M. Hu, "Statistical analysis of deformation laws of deep foundation pits in collapsible loess," *Arabian Journal for Science and Engineering*, vol. 44, pp. 8347–8360, 2019.

[11] C. Y. Ou, H. Pio-Go, and C. Dar-Chang, "Characteristics of ground surface settlement during excavation," *Canadian Geotechnical Journal*, vol. 30, pp. 758–767, 1993.

[12] J. H. Wang, Z. H. Xu, and W. D. Wang, "Wall and ground movements due to deep excavations in shanghai soft soils," *Journal of Geotechnical and Geoenvironmental Engineering*, vol. 136, pp. 985–995, 2010.

[13] I. H. Wong, T. Y. Poh, and H. L. Chuah, "Performance of excavations for depressed expressway in Singapore," *Journal of Geotechnical Engineering*, vol. 123, pp. 617–625, 1997.

[14] H. W. Ying, K. Cheng, L. S. Zhang, C. Y. Ou, and Y. W. Yang, "Evaluation of excavation-induced movements through case histories in Hangzhou," *Engineering Computations*, vol. 37, pp. 1993–2016, 2020.

[15] Y. Q. Zhang, M. G. Lia, J. H. Wang, J. J. Chen, and Y. F. Zhu, "Field tests of pumping- recharge technology for deep confined aquifers and its application to a deep excavation," *Engineering Geology*, vol. 228, no. 10, pp. 249–259, 2017.

[16] P. Jamsawang, S. Jamnam, P. Jongpradist, P. Tanseng, and S. Horpibulsuk, "Numerical analysis of lateral movements and strut forces in deep cement mixing walls with top-down construction in soft clay," *Computers and Geotechnics*, vol. 88, pp. 174–181, 2017.

[17] G. B. Liu, R. J. Jiang, C. W. W. Ng, and Y. Hong, "Deformation characteristics of a 38 m deep excavation in soft clay," *Canadian Geotechnical Journal*, vol. 48, pp. 1817–1828, 2011.

[18] Y. Tan and M. Li, "Measured performance of a 26 m deep top-down excavation in downtown Shanghai," *Canadian Geotechnical Journal*, vol. 48, pp. 704–719, 2011.

[19] H. Xiao, S. Zhou, and Y. Sun, "Wall deflection and ground surface settlement due to excavation width and foundation pit classification," *KSCE Journal of Civil Engineering*, vol. 23, pp. 1–11, 2019.

[20] H. W. Ying, C. W. Ng, G. B. Liu, and T. Liu, "Three-dimensional deformation behaviour of a multi-propped excavation at a "greenfield" site at shanghai soft clay," *Tunnelling and Underground Space Technology*, vol. 45, pp. 249–259, 2015.

[21] C. Chheng and S. Likitlersuang, "Underground excavation behaviour in Bangkok using three-dimensional finite element method," *Computers and Geotechnics*, vol. 95, pp. 68–81, 2018.

[22] Y. P. Dong, H. J. Burd, and G. T. Houlsby, "Finite element parametric study of the performance of a deep excavation," *Soils and Foundations*, vol. 58, pp. 729–743, 2018.

[23] A. T. C. Goh, F. Zhang, W. G. Zhang, Y. M. Zhang, and H. L. Liu, "A simple estimation model for 3D braced excavation wall deflection," *Computers and Geotechnics*, vol. 83, pp. 106–113, 2017.

[24] B.-C. B. Hsiung, K.-H. Yang, W. Aila, and L. Ge, "Evaluation of the wall deflections of a deep excavation in Central Jakarta using three-dimensional modeling," *Tunnelling and Underground Space Technology*, vol. 72, p. 84, 2018.

[25] Z. Y. Orazalin, A. J. Whittle, and M. B. Olsen, "Three-dimensional analyses of excavation support system for the stata center basement on the MIT campus," *Journal of Geotechnical and Geoenvironmental Engineering*, vol. 141, Article ID 0505001, 2015.

[26] L. Zdravkovic, D. M. Potts, and H. D. St John, "Modelling of a 3D excavation in finite element analysis," *Géotechnique*, vol. 55, pp. 497–513, 2005.

[27] R. A. Forth, "Groundwater and geotechnical aspects of deep excavations in Hong Kong," *Engineering Geology*, vol. 72, no. 3-4, pp. 253–260, 2004.

[28] C. Y. Ou, J. T. Liao, and W. L. Cheng, "Building response and ground movements induced by a deep excavation," *Géotechnique*, vol. 50, pp. 209–220, 2000b.

[29] M. Lu, P. Li, B. Chen, and Y. Chen, "Computer simulation of the dynamic layered soil pile-structure interaction system," *Canadian Geotechnical Journal*, vol. 42, pp. 742–751, 2005.

[30] H. W. Ying, Y. W. Yang, and X. Y. Xie, "Field Performance of a Deep Multi-Strutted Excavation in Hangzhou Soft Clays," *Advanced Materials Research*, vol. 243, pp. 2324–2327, 2011.

[31] G. W. Clough and T. D. O'Rourke, "Construction induced movements of in situ wall," *Geotechnical Special Publication*, vol. 25, pp. 439–470, 1990.

[32] R. B. Peck, "Deep excavations and tunnelling in soft ground," in *Proceedings of the 7th International Conference on Soil Mechanics and Foundation Engineering*, pp. 225–290, Mexico City, 1969.

[33] G. W. E. Milligan, "Soil deformations near anchored sheet-pile walls," *Géotechnique*, vol. 33, pp. 41–55, 1983.

[34] J. E. Bowles, *Foundation Analysis and Design*, McGraw-Hill, New York, 1988.

[35] A. I. Mana and G. W. Clough, "Prediction of movements for braced cuts in clay," *Journal of the Soil Mechanics and Foundations Division*, vol. 107, pp. 759–777, 1981.

[36] C. Moormann, "Analysis of wall and ground movements due to deep excavations in soft soil based on a new worldwide database," *Soils and Foundations*, vol. 44, pp. 87–98, 2004.
[37] C. W. W. Ng, D. B. Rigby, G. H. Lei, and S. W. L. Ng, "Observed performance of a short diaphragm wall panel," *Géotechnique*, vol. 49, pp. 681–694, 1999.
[38] S. Likitlersuang, C. Surarak, D. Wanatowski, E. Oh, and A. Balasubramaniam, "Finite element analysis of a deep excavation: a case study from the Bangkok MRT," *Soils and Foundations*, vol. 53, pp. 756–773, 2013.
[39] C. Y. Ou, *Deep Excavation Engineering: Theory and Practice*, Science and technology books, Taipei, 2006.
[40] E. H. Y. Leung and C. W. W. Ng, "Wall and ground movements associated with deep excavations supported by cast in situ wall in mixed ground conditions," *Journal of Geotechnical and Geoenvironmental Engineering*, vol. 133, pp. 129–143, 2007.